ature distribution provide enough information for system optimization.

REFERENCES

1. D.R. MacFarlane and M. Fragoulis, Theory of devitrification in multicomponent glass forming systems under diffusion control, Physical chemistry, Glasses 27 (1986), 228–243.
2. P. Boutron and P. Mehl, Theoretical prediction of devitrification tendency: determination of critical warming rate without using finite expansions, Cryobiol 27 (1990), 359–377.
3. D.E. Pegg, M.C. Wusteman, and S. Boylan, Fractures in cryopreserved elastic arteries, Cryobiol 34 (1997), 183–192.
4. M.P. Rubinsky, E.G. Cravalho, and B. Mikik, Thermal stress in frozen organs, Cryobiol 17 (1980), 66–73.
5. M.P. Robinson and D.E. Pegg, Rapid electromagnetic warming of cells and tissues, IEEE Trans Biomed Eng 46 (1999), 1413–1425.
6. M.P. Robinson, D.E. Pegg, and M.C. Wusteman, Electromagnetic heating of vitrified tissues: influence of dielectric properties on rewarming characteristics, Cryobiol 43 (2001), 346–355.
7. M.P. Robinson, Electromagnetic rewarming of cryopreserved tissues: effect of choice of cryoprotectant and sample shape on uniformity of heating, Phys Med and Biol 47 (2002), 2311–2325.
8. C.C. Lu, D.Y. Gao, and H.Z. Li, Analysis of microwave rewarming of cryopreserved tissues, IEEE Antennas Propagat Soc Int Symp Dig 2 (2000), 1068–1071.
9. F. Toress and B. Jecko, Complete FDTD analysis of microwave heating processes in frequency-dependent and temperature-dependent media, IEEE Trans Microwave Theory Techniques 45 (1997), 108–116.
10. J.G. Maloney, A simple FDTD model for transient excitation of antenna by transmission lines, IEEE Trans Antennas Propagat 42 (1994), 289–293.
11. S. Dey and R. Mittra, A modified locally conformal finite-difference time domain algorithm for modeling three dimensional perfectly conducting objects, Microwave Opt Technol Lett 17 (1998), 348–352.
12. S. Dey and R. Mittra, A conformal finite-difference time domain technique for modeling cylindrical dielectric resonators, IEEE Trans Microwave Theory Tech 47 (1999), 1737–1739.
13. P. Monk and E. Suli, A convergence analysis of Yee's scheme on non-uniform grids, SIAM J Numer Analysis 31 (1994), 393–412.
14. M.J. Richardson, Application of differential scanning calorimetry in the determination of specific heat, Compendium of thermophysical property measurement methods, Plenum, New York, (1984), pp. 669–685.
15. R.E. Collin, Field theory of guided waves, IEEE Press, New York, 1991.

PIFA LOADED WITH ARTIFICIAL MAGNETIC MATERIAL: PRACTICAL EXAMPLE FOR TWO UTILIZATION STRATEGIES

Pekka Ikonen, Stanislav Maslovski, and Sergei Tretyakov
Radio Laboratory/SMARAD
Helsinki University of Technology
P.O. Box 3000
FI-02015 TKK, Finland

Received 21 January 2005

ABSTRACT: *In this paper, we experimentally investigate the effect of artificial magnetic material loading on the radiation properties of a planar inverted F-antenna (PIFA). We introduce two principal strategies for the utilization of the magnetic material with planar antennas. It is shown that a dramatic bandwidth enhancement is achievable when the material is utilized in its resonant regime. In addition, it is experimentally proven that at frequencies below the material resonance, the load can be considered as a paramagnetic material, thus enabling efficient size miniaturization.* © 2005 Wiley Periodicals, Inc. Microwave Opt Technol Lett 46: 205–210, 2005; Published online in Wiley InterScience (www.interscience.wiley.com). DOI 10.1002/mop.20946

Key words: *PIFA; artificial magnetic materials; metasolenoid; miniaturization*

1. INTRODUCTION

It is expected that the enormous growth of the traffic load in wireless networks will continue in the near future [1]. The growing trend in the communications industry is to favor smaller-size handheld devices. However, the necessity of size miniaturization should not mean the loss of capability to fulfill the capacity requirements set by communications systems. This is especially important with antennas; as the size of an antenna is miniaturized, it is important that the bandwidth of the antenna is retained. This ensures, for example, that the same amount of information can be transferred with the modified, smaller-size antenna.

One of the most common ways to achieve size miniaturization of a planar antenna is to load the volume under the patch element with different materials [2]. This usually lowers the resonant frequency; by decreasing the size of the patch element, the operational frequency can be tuned back to the original frequency. The result is a smaller-size antenna; however, the drawback with most of the loading methods introduced in the literature is a more narrow fractional bandwidth and/or suffered radiation efficiency.

During the first heyday of so-called metamaterials [3, 4], electromagnetically exotic materials gained a lot of interest among antenna designers. Magnetodielectric substrates [5, 6], ferromagnetic substrates [7], and high-permittivity materials [8] have been proposed to be utilized in antenna miniaturization and performance optimization. Electromagnetic band-gap (EBG) materials [9] and their utilization with planar antennas have been extensively studied (see, for example, [10–13]). Recently, artificial magnetic materials [14, 15] were proposed as a mean to improve the performance of planar antennas [16, 17].

Another direction for the optimization of planar antennas is to fix the volume of an antenna and try to increase the bandwidth. Commonly used bandwidth enhancement techniques include the utilization of conventional resonators [18] and parasitic patches [19, 20], as well as the modification of the shape and the size of the patch element [21, 22]. In most cases the wider bandwidth is achieved with the cost of increased antenna size (consider, for example, parasitic patches).

In the present work, we briefly revise the basic principles behind the aim to achieve size miniaturization of planar antennas with different material loadings. The *metasolenoid* [15] is chosen as an example unit cell of a magnetic material, and it is used to load the volume under a PIFA patch. We characterize two different

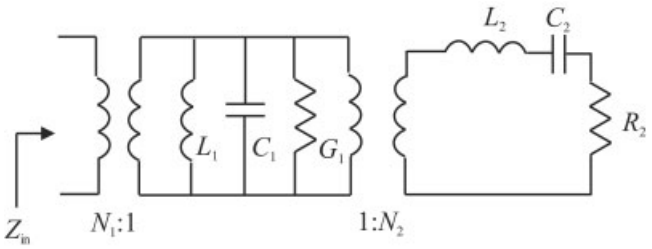

Figure 1 Circuit model for the PIFA and the chassis

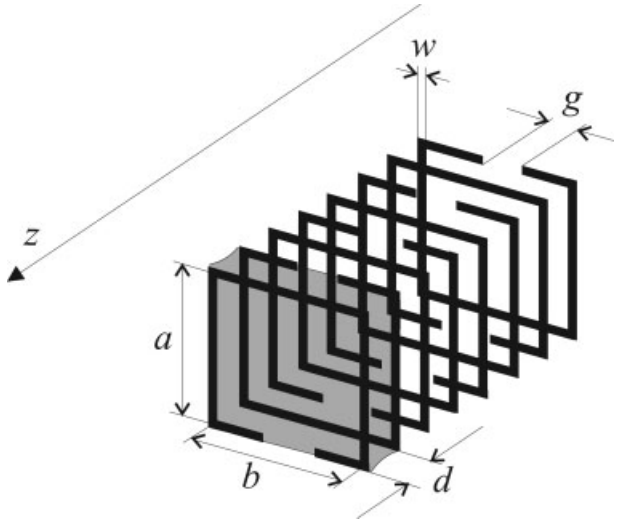

Figure 2 The metasolenoid [15]

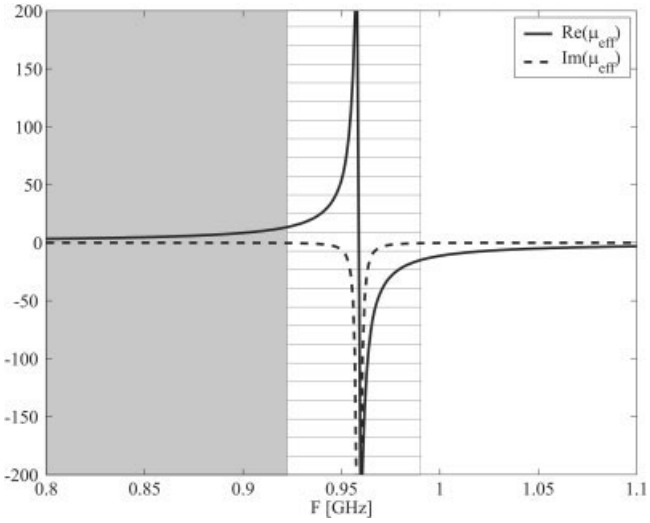

Figure 3 Typical dispersive behavior for μ_{eff} of a medium densely filled with metasolenoids (the part with lines denotes the resonant region, the grey part denotes the effective material region)

frequency regions for different utilization principles: In the first scenario we utilize the metasolenoids in their resonant regime and construct a compact size multiresonant antenna. In the second case the metasolenoids are utilized at frequencies below their resonant frequency and function as an artificial material loading.

2. MATERIAL LOADING OF PLANAR ANTENNAS

2.1. Known Limitation of Electrically Small Antennas and the Figure of Merit

An antenna is characterized by many important parameters, but it is possible to define a universal parameter that determines which (electrically small) antenna is "better" in terms of its size and bandwidth. This can be done using the concept of the minimum quality factor of small antennas. It is well known that there is a fundamental limitation on the minimum quality factor of small antennas [23, 24]. For a small antenna radiating as an electric or magnetic dipole, and contained in a sphere of radius a, the quality factor is limited by the value of

$$Q > \frac{1}{(k_0 a)^3}, \tag{1}$$

where k_0 is the free-space wavenumber ($k_0 a \ll 1$). We can observe that for antennas operating at a given frequency the product $Qa^3 \sim QV$ (with V the antenna volume in the limiting case) is restricted by the basic physics, and the limit depends only on the frequency. Thus, when comparing two antennas operating at the same frequency, we can conclude that the antenna characterized by a smaller value of QV is better in the sense of its size and bandwidth. Similarly, when comparing two antennas of the same volume V and different working frequencies and quality factors, the figure of merit is the product QF_{res}^3, where F_{res} is the resonant frequency of the two antennas. The smaller this value, the closer we come to the fundamental limit of the antenna performance. The aim of the optimization procedure is to minimize the parameters QV or QF_{res}^3.

TABLE 1 Metasolenoid Dimensions (See Fig. 2 for Definition)

a mm	b mm	w mm	g mm	d mm	ε_r
3.5	3.5	0.4	1.0	0.127	$2.20 - j0.002$*

* ϵ_r is the permittivity of the host substrate.

2.2. PIFA Circuit Model

The PIFA [25] is one of the most common internal antenna structures used by the biggest mobile-phone manufacturers. The equivalent circuit of a PIFA, taking into account the effect of the mobile phone chassis, is presented in Figure 1 [26]. The parallel resonant circuit represents the patch element, which is coupled to the chassis represented by the series-resonant circuit.

There are several directions for the optimization of electrically small antennas of mobile terminals. One of the directions is an effective excitation of the chassis with the so-called coupling elements [26, 27]. However, this solution is not always possible or preferable. In this paper, we consider a patch element lying above an infinite ground plane and neglect the series resonant circuit in the equivalent circuit model.* This approach is chosen to clarify the fundamental effect of different material loadings.

It is known from basic circuit theory that the quality factor of a parallel-resonant circuit is of the following form (the notations refer to Fig. 1):

$$Q = R_1 \sqrt{\frac{C_1}{L_1}}, \tag{2}$$

where Q is the quality factor of the resonator, $R_1 = 1/G_1$ is the resistance representing the losses in the resonator, and C_1 and L_1 are the capacitance and the inductance of the resonator, respectively. Thus, we can readily write the proportionality for the bandwidth and the resonant frequency of a parallel-resonant circuit as follows:

$$BW \propto \sqrt{\frac{L_1}{C_1}}, \; F_{\text{res}} \propto \frac{1}{\sqrt{L_1 C_1}}. \tag{3}$$

From such a simplistic circuit model we can draw the known observation [2, 5, 16] that by increasing the inductance of the

* Basically, by doing this we are optimizing the radiation properties of the patch element.

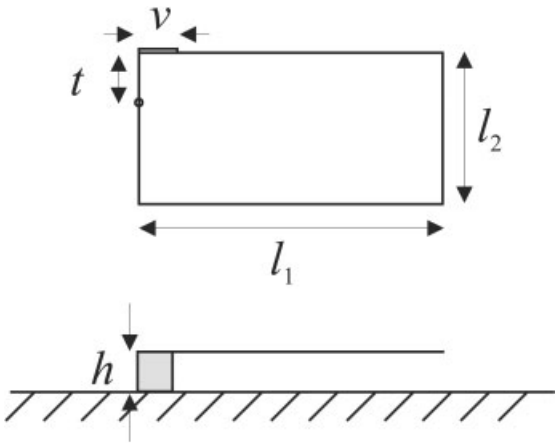

Figure 4 Geometry of the PIFA used in the measurements

setup, for example, by an appropriate loading of the volume under the patch with a magnetic material, the resonant frequency of the antenna decreases, but the reduction of the bandwidth can at the same time be (partly) compensated. Electrical (capacitive) loading, that is, loading the antenna volume with capacitive loads (ordinary metal pieces, dielectrics, and so on) also lowers the resonant frequency, but usually the bandwidth also becomes narrower [2, 8]. The utilization of high-permittivity materials in size miniaturization usually leads also to strong electromagnetic coupling between the patch and the metal ground behind the substrate, excitation of surface waves, and difficulties in the antenna impedance matching [11].

3. THE CHOSEN ARTIFICIAL MAGNETIC PARTICLE

It is well-known that natural magnetic materials loose their magnetic properties at microwave and millimeter-wave frequencies. This is the main reason why magnetic loading of antennas is still not commonly used at microwave frequencies. The concept of artificial magnetism was actively launched only a few years ago after the discovery of metamaterials (see, for example, [14, 15]).[†] Simply stated, artificial magnetic materials are composite structures with conducting inclusions of complex shapes. Magnetism is created without magnetic constituents. Usually, single particles (unit cells) that constitute the artificial magnetic material are loop-shaped resonating particles.

The chosen unit cell used to construct an artificial magnetic material is shown in Figure 2. The particle is called a metasolenoid. A detailed analysis of the metasolenoid can be found in [15]. The dimensions of the metasolenoid samples used in the measurements are presented in Table 1. When the small unit cells (metasolenoids) are positioned in close proximity to each other, the structure formed in this way can be considered as a piece of a certain medium characterized by effective material parameters ε_{eff} and μ_{eff}.** For example, when we put many properly designed metasolenoids under the patch element of a PIFA, we can physically think that the volume under the patch is occupied by a block of medium (material) characterized by a certain μ_{eff}. If the value of μ_{eff} exceeds unity at the operational frequency, the material loading can be considered as a paramagnetic material; thus, we have achieved inductive loading, which is necessary for efficient size miniaturization.

[†] Although this has been known since the 1950s (Schelkunoff).
** The wavelength has to be large compared to the element and particle size [28].

TABLE 2 Dimensions of the Patch Elements

Patch 1				
l_1 mm	l_2 mm	v mm	t mm	h mm
40.0	20.0	5.0	3.0	6.50
Patch 2				
l_1 mm	l_2 mm	v mm	t mm	h mm
45.0	30.0	5.0	3.0	6.50

The dispersive behavior for the μ_{eff} of a medium densely filled with the introduced size metasolenoids is presented in Figure 3. Because the unit cell (metasolenoid) that constitutes the medium is a resonator, the medium is also of resonant type (the resonant region corresponds to the frequencies where the absolute value of μ_{eff} is very large, see Fig. 3). If a PIFA having metasolenoids under its patch resonates near 0.95 GHz (Fig. 3), then the metasolenoids would be excited very strongly, and rather than being considered as a magnetic material loading, they would behave as parasitic resonators. But, if we instead design a PIFA to resonate around 0.85 GHz with the particles under the patch, we would no longer utilize the resonant regime of the medium, since at 0.85 GHz $\text{Re}\{\mu_{\text{eff}}\}$ is almost constant, yet larger than unity. Thus, in the latter case the particles behave as a magnetic material occupying the volume under the PIFA patch.

For the following measurements, we construct two PIFAs. In the first case (case I), the resonant frequency of the PIFA with the metasolenoids under the patch corresponds to the resonance of the metasolenoid. In the second case (case II), the frequency of the loaded PIFA is considerably below the resonance of the metasolenoid.

4. MEASURED RESULTS

4.1. Measurement Setup

To eliminate the effect of the finite ground plane, all the measurements were performed using a large 30 × 30 cm metal ground

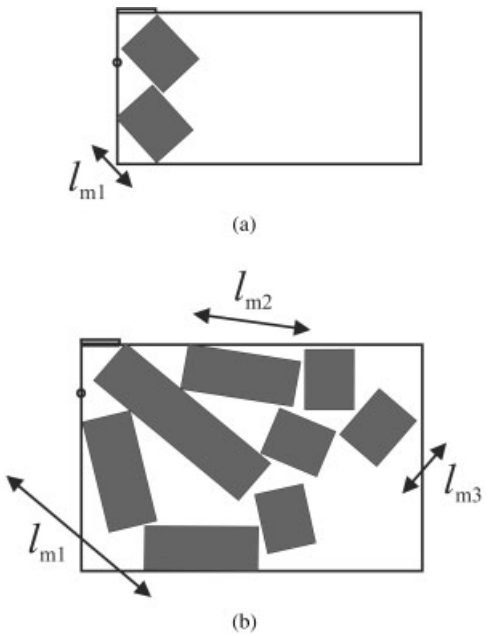

Figure 5 Positioning of the metasolenoids under the patch elements: metasolenoids under the patch element for (a) case I (l_{m1} = 7.5 mm); (b) Case II (l_{m1} = 25.0 mm, l_{m2} = 15.0 mm, l_{m3} = 7.5 mm)

TABLE 3 Measured Parameters for Case I

Loading	F_{res} GHz	$BW\|_{-6dB}$ [%]	$BW\|_{-9.5dB}$ [%]	η [%]	Q_0	$Q_0F_{res}^3$
Air	1.30	4.5	2.7	94	27.2	59.8
Reference blocks	1.29	4.4	2.6	93	27.6	59.3
Metasolenoids	1.26	5.4	4.3	90, 90, 88*	22.1	45.8

* The three values correspond to the three resonant peaks shown in Fig. 6.

plane. The patch is located in the middle of the ground. In the measurements, we utilized the manufactured metasolenoid samples introduced in [15]. Since the manufactured metasolenoids are resonating at around 1.2 GHz, we designed two different PIFA patches: the first patch (patch 1) was designed to resonate at approximately 1.2 GHz (when the metasolenoids are positioned under the patch), and the second patch was designed to resonate well below the resonance of the metasolenoids. A schematic illustration of the patch geometry is depicted in Figure 4. Table 2 introduces the dimensions of the two patches.

4.2. Definitions for Data Processing

In this subsection, we define the procedure for determining the figures of merit used in the performance comparison. The coupling coefficient T describes the quality of the matching between the source and the resonator, given by

$$T = \frac{Y_s}{G}, \tag{4}$$

where Y_s is the admittance of the feed line and $G = 1/R$ is the conductance of the parallel resonator. Let us assume that the criterion for the maximum VSWR inside of the band of interest is

$$\text{VSWR} \leq S. \tag{5}$$

In this case, the fractional bandwidth can be expressed as

$$BW_r = \frac{1}{Q_0}\sqrt{\frac{(TS-1)(S-T)}{S}}, \tag{6}$$

where Q_0 is the unloaded quality factor of the parallel resonator. To compare the performance of the radiator in different cases (with different loadings), we fix the volume of the antenna and use the product $Q_0F_{res}^3$ as a figure of merit. The resonant frequency is given in GHz. The unloaded quality factor is solved from Eq. (6), and a 6-dB return loss level is used in the calculation of the figure of merit. The radiation efficiencies have been measured using the Wheeler cap method and calculated as

$$\eta = \left(1 - \frac{R_0}{R}\right) \times 100, \tag{7}$$

where R_0 is the real part of the input impedance of the covered antenna at resonance, and R is the real part of the antenna impedance without the covering, at the resonance.

4.3. Case I: Metasolenoids as Parasitic Resonators

In the first case, the metasolenoids are utilized in their resonant regime. Patch 1 is used in the measurements. Two metasolenoids are positioned under the patch, as depicted in Figure 5(a). The orientation of the metasolenoids has been experimentally tuned to obtain a suitable coupling level between the metasolenoids and the patch element in order to maximize the achieved bandwidth. The measured S_{11}-parameter is depicted in Figure 6. The reference blocks are dielectric blocks made out of the host material of the metasolenoid (they are of the same size as the metasolenoids). Observing the metasolenoids, we can see that there are three distinct resonant peaks, one of which corresponds to the resonance of the patch element and two of which correspond to the resonance of the metasolenoids. These three resonant peaks can be conveniently combined with suitable coupling, thus resulting in a compact size (the volume of the antenna structure is not increased) wideband antenna. The measured parameters are given in Table 3. With a multiresonant antenna, the radiation efficiency cannot be readily linked to the measured input impedance (when using the Wheeler cap method). Moreover, in the multiresonant case, it can be highly complicated to define whether the loss resistance is in parallel or in series with the rest of the circuit (the requirement for use of the Wheeler cap method). In many cases, there can be both series and parallel resistance representing the losses. However, to obtain an estimate of the radiation efficiency, we calculate the efficiency using Eq. (7) at three discrete frequencies, corresponding to the resonant peaks shown in Figure 6.

4.4. Case II: Metasolenoids as Material Loading

In the second measurement case, the metasolenoids are utilized at frequencies well below their resonant frequency. Patch 2 is used in the measurements. The metasolenoids are positioned under the patch, as depicted in Fig. 5(b). The orientation of the metasolenoids has been experimentally tuned so that the metasolenoids occupy the volume as evenly as possible, while still collecting most of the circulating flux. The achieved volume filling ratio V_r (under the patch element) is 14%.[4] Using the effective medium model presented in [15], we estimate that the effective permeability of a medium filled with the metasolenoids, and having $V_r = 0.14$, is approximately 1.4 at 0.85 GHz. Thus, we can expect to see the effect of magnetic-material loading when calculating the figure of merit.

The measured S_{11}-parameter is depicted in Figure 7. Small ripple around 1.15 GHz corresponds to some higher-order weakly excited modes of the metasolenoids. The measured parameters are given in Table 4. We can clearly see from Figure 7 and Table 4 that both loading materials (dielectrics and metasolenoids) reduce the resonant frequency of the PIFA rather remarkably. The metasolenoids lower the resonant frequency noticeably more, as compared to the dielectric loading. This may simply be due to the fact that in addition to having a dielectric substrate under the patch, we also have metal inclusions under the patch. There is a possibility that the inclusions act only as ordinary metal pieces (capacitive loads) and cause an additional reduction in the resonant frequency. On the other hand, based on the presented discussion, the metallic inclusions can also act as an effective magnetic material when, in addition to lowering the resonant frequency of the antenna, we can better retain the fractional bandwidth.

[4] The schematic illustration presented in Figs. 5(a) and 5(b) takes into account the laminate surrounding the metasolenoid rings.

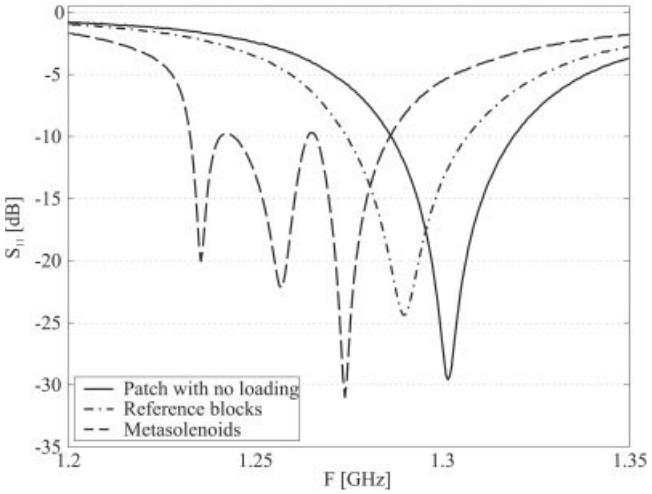

Figure 6 Measured S_{11}-parameter for case I

The calculated figures of merit (see Table 4) validate the expectation of the metasolenoids acting as a magnetic material: as the dielectric (capacitive) loading is used, the resonant frequency is lowered, but the bandwidth suffers even more strongly. This is seen as an increased figure of merit. The figure of merit is minimized in the case of the metasolenoid loading, implying that the particles act as an effective magnetic material and hence result in inductive loading (if the volume filling ratio was bigger, a stronger difference would be seen). The measured figure of merit also implies that we are closer to the fundamental antenna limit with the metasolenoid loading. The relatively high radiation efficiency measured in this work proves the feasibility of the proposed loading technique.

5. DISCUSSION

For efficient data transmission, it is desirable that the antenna be as wideband as possible. Electrically small antennas are known to be inherently narrowband and relatively inefficient radiators. However, the aim in the communications industry is still towards smaller size devices. This means that the antenna size should be further miniaturized. We are facing a clear dilemma: somehow the antenna size should be decreased, but at the same time the device should be capable of transmitting more and more data with a smaller-size antenna.

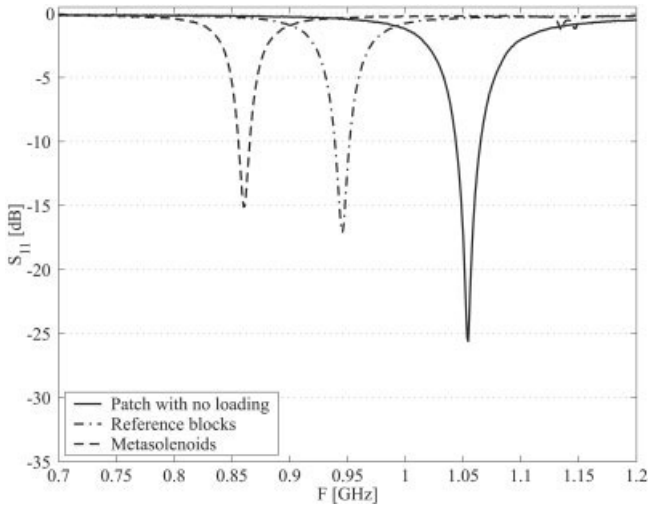

Figure 7 Measured S_{11}-parameter for case II.

TABLE 4 Measured Parameters for Case II

Loading	F_{res} GHz	$BW\|_{-6dB}$ [%]	$BW\|_{-9.5dB}$ [%]	η [%]	Q_0	$Q_0 F_{res}^3$
Air	1.05	3.6	2.2	84	34.3	40.2
Reference blocks	0.95	2.5	1.5	74	51.0	43.2
Metasolenoids	0.86	2.2	1.3	70	59.4	37.8

It has been discussed that conventional (capacitive) loading techniques are not desirable ways to achieve the antenna miniaturization. We are able to lower the resonant frequency of the antenna, but bandwidth is lost. Effective inductive loading would enable a decrease in the resonant frequency while retaining the bandwidth. Artificial magnetic materials are proposed as inductive loading (in contrast to capacitive loading) in order to achieve efficient miniaturization. In this paper, we have briefly revised the basic principles behind the aim to achieve size miniaturization of planar antennas with different material loadings. Two utilization strategies have been introduced for resonant-type magnetic materials and the discussion has been validated by the experiments. It has been shown that the utilization of the resonant regime of the material enables a dramatic bandwidth enhancement. On the other hand, artificial magnetic material utilized at frequencies below its resonance can enable efficient size miniaturization of a planar antenna.

REFERENCES

1. W. Webb, The future of wireless communications, Artech House, Boston, MA, 2001.
2. O. Edvardsson, On the influence of capacitive and inductive loading on different types of small patch/PIFA structures for use on mobile phones, ICAP Int Conf Antennas Propagat, Manchester, UK, 2001, pp. 762–765.
3. J.B. Pendry, A.J. Holden, D.J. Robbins, and W.J. Stewart, Magnetism from conductors and enhanced nonlinear phenomena, IEEE Trans Microwave Theory Tech 47 (1999), 2075–2084.
4. D.R. Smith, W.J. Padilla, D.C. Vier, S.C. Nemat-Nasser, and S. Schultz, Composite medium with simultaneously negative permeability and permittivity, Phys Rev Lett 84 (2000), 4184–4187.
5. R.C. Hansen and M. Burke, Antenna with magneto-dielectrics, Microwave Opt Technol Lett 26 (2000), 75–78.
6. S. Yoon and R.W. Ziolkowski, Bandwidth of a microstrip patch antenna on a magneto-dielectric substrate, IEEE Antennas Propagat Soc Int Symp, Columbus, OH, 2003, pp. 297–300.
7. A.D. Brown, J.L. Volakis, L.C. Kempel, and Y.Y. Botros, Patch antennas on ferromagnetic substrates, IEEE Trans Antennas Propagat 47 (1999), 26–32.
8. Y. Hwang, Y.P. Zhang, G.X. Zheng, and T.K.C. Lo, Planar inverted-F antenna loaded with high permittivity material, Electron Lett 31 (1995), 1710–1712.
9. D. Sievenpiper, L. Zhang, R.F. Jimenez Broas, N.G. Alexòpolous, and E. Yablonovitch, High-impedance electromagnetic surfaces with a forbidden frequency band, IEEE Trans Microwave Theory Tech 47 (1999), 2059–2074.
10. M. Qiu and S. He, High directivity patch antenna with both photonic bandgap substrate and photonic bandgap cover, Microwave Opt Technol Lett 30 (2001), 41–44.
11. K. Buell, D. Cruickshank, H. Mosallaei, and K. Sarabandi, Patch antenna over RIS substrate: A novel miniaturized wideband planar antenna design, IEEE Antennas Propagat Soc Int Symposium, Columbus, OH, 2003, pp. 269–272.
12. H. Mosallaei and K. Sarabandi, Antenna miniaturization and band-

width enhancement using a reactive impedance substrate, IEEE Trans Antennas Propagat 52 (2004), 2403–2414.
13. Y. Zhao, Y. Hao, and C.G. Parini, Radiation properties of PIFA on electromagnetic bandgap substrates, Microwave Opt Technol Lett 44 (2005), 21–24.
14. M.V. Kostin and V.V. Shevchenko, Artificial magnetics based on double circular elements, Proc Bianisotropics'94, Périgueux, France, 1994, pp. 49–56.
15. P. Ikonen, S.I. Maslovski, I.A. Kolmakov, and S.A. Tretyakov, New artificial high permeability material for microwave applications, Progress Electromagn Res Symp, Pisa, Italy, 2004, pp. 485–488.
16. K. Buell, H. Mosallaei, and K. Sarabandi, Embedded-circuit magnetic metamaterial substrate performance for patch antennas, IEEE Antennas Propagat Soc Int Symp, Monterey, CA, 2004, pp. 1415–1418.
17. M.K. Kärkkäinen, S.A. Tretyakov, and P. Ikonen, Numerical study of a PIFA with dispersive material fillings, Microwave Opt Technol Lett 45 (2005), 5–8.
18. L.L. Rauth, J.S. McLean, K.R. Dorner, J.R. Casey, and G.E. Crook, Broadband, low-profile antenna for portable data terminal, IEEE Antennas Propagat Soc Int Symp, Montreal, Canada, 1997, pp. 438–441.
19. F.-R. Hsiao and K.-L. Wong, Compact planar inverted-F patch antenna for triple-frequency operation, Microwave Opt Technol Lett 33 (2002), 459–462.
20. K.L. Virga and Y. Rahmat-Samii, Low-profile enhanced-bandwidth PIFA antennas for wireless communications packaging, IEEE Trans Microwave Theory Tech 45 (1997), 1879–1888.
21. P. Salonen, M. Keskilammi, and M. Kivikoski, Single-feed dual-band planar inverted-F antenna with U-shaped slot, IEEE Trans Antennas Propagat 48 (2000), 1262–1264.
22. D.M. Pozar, Microstrip antennas, Proc IEEE 80 (1992), 79–91.
23. H.A. Wheeler, Fundamental limitations of small antennas, Proc IRE 35 (1947), 1479–1484.
24. R.C. Hansen, Fundamental limitations in antennas, Proc IEEE 69 (1981), 170–182.
25. T. Taga and K. Tsunekawa, Performance analysis of a built-in planar inverted-F antenna for 800-MHz band portable radio units, IEEE J Sel Areas Commun 5 (1987), 921–929.
26. P. Vainikainen, J. Ollikainen, O. Kivekäs, and I. Kelander, Resonator-based analysis of the combination of mobile handset antenna and chassis, IEEE Trans Antennas Propagat 50 (2002), 1433–1444.
27. J. Villanen, J. Ollikainen, O. Kivekäs, and P. Vainikainen, Compact antenna structures for mobile handsets, Proc IEEE 58th Vehic Technol Conf, Orlando, FL, 2003, pp. 40–44.
28. S. Tretyakov, Analytical modelling in applied electromagnetics, Artech House, Norwood, MA, 2003.

STEADY-STATE ANALYSIS OF A DIRECTIONAL SQUARE LATTICE BAND-EDGE PHOTONIC CRYSTAL LASERS

Rogério M. Cazo,[1] Carmem L. Barbosa,[1] Haroldo T. Hattori,[2] and Vitor M. Schneider[3]
[1] Photonics Division
Instituto de Estudos Avançados-CTA
São José dos Campos SP, Brazil
[2] LEOM-CNRS-Ecole Centrale de Lyon
36 Avenue de Collongue
69134 Ecully, France
[3] 19 Eagle Drive, Apt. 202
Painted Post, NY 14870

Received 19 January 2005

ABSTRACT: *The original square-lattice band-edge structure emitted light in different directions. In a recent paper [18], we have improved the directivity of these structures by using a honeycomb photonic crystal to shield the original structure. This has improved the performance of such devices, in such a way that light can be coupled directionally to a large waveguide. In this paper, we present a steady-state analysis of the performance of this directive device and study the amount of power which can be coupled into the waveguide, analyzing its performance as an in-plane emitter and the limitations caused by vertical losses.* © 2005 Wiley Periodicals, Inc. Microwave Opt Technol Lett 46: 210–214, 2005; Published online in Wiley InterScience (www.interscience.wiley.com). DOI 10.1002/mop.20947

Key words: *photonic crystal devices; integrated optics devices; diode lasers*

1. INTRODUCTION

Photonic crystals (PhCs) are periodic structures of high index contrast, which present the property of forbidding the propagation of light in a certain wavelength range, a property that can be used to manipulate the flow of light in different ways. A complete photonic bandgap for all directions and polarizations can be obtained using 3D PhCs, but their fabrication processes are not very well controlled and they tend to have many imperfections. On the other hand, fabrication of bidimensional (2D) PhCs has been well established and a multitude of devices have already been produced, such as filters [1–3], waveguide bends and branches [4, 5], lasers [6–18], and so forth.

One possible major contribution of PhCs will be in the area of compact and efficient laser devices. PhCs allow the confinement of light in small volumes, which can change their optical-emission properties, thus allowing both enhancement and inhibition [15]. The most common configurations for these devices are defect-mode [6–9], surface-emitting [10–12], and band-edge [13–14, 16–18] lasers. Defect-mode lasers can have quality factors (Q) as high as 10,000 and low threshold currents, but as argued by Ohnishi et al. [12], broad-area lasers such as band-edge lasers have the advantage of providing larger output power, better heat dissipation, and narrower beam-divergence.

Band-edge lasers operate at the edges of the first Brillouin zone, at high-symmetry points (for example, the X point in a square lattice of air holes). In many cases, the high-symmetry points of a given mode present extreme points in their band diagrams. At these extreme points, the group velocity of a given mode can be made very small, that is, the average lifetime of the photons in the active area can be made large, thus significantly reducing the size of the device [13]. Band-edge lasers can be considered as the photonic-crystal equivalents to DFB lasers. Actually, band-edge lasers in triangular [13] and square [14] lattices of air holes have been analyzed recently. However, thus far these devices have emitted light in different directions.

Our band-edge laser will have a main PhC that consists of square lattices of air holes in a semiconductor slab and will operate at the X point in the first Brillouin zone. Without loss of generality, we will restrict our attention to the transverse electric (TE) modes (using the same convention as in [4]), and the operating mode will be the first one in the valence band. Initially, we describe the original and modified structures and, subsequently we shall present a steady-state analysis of the directive laser device, including the effects of vertical losses. These effects were also commented upon in a recent paper by Topol'ancik et al. [17], in which laser sources with defect-cavities coupled light to W1 waveguides. In this recent paper, it was shown that the coupling of light to narrow waveguides was severely degraded by vertical losses (a fact that explained why the coupled power into a W1 waveguide was in the range of tens of pW).

射 频 和 天 线 设 计 培 训 课 程 推 荐

易迪拓培训(www.edatop.com)由数名来自于研发第一线的资深工程师发起成立，致力并专注于微波、射频、天线设计研发人才的培养；我们于 2006 年整合合并微波 EDA 网(www.mweda.com)，现已发展成为国内最大的微波射频和天线设计人才培养基地，成功推出多套微波射频以及天线设计经典培训课程和 ADS、HFSS 等专业软件使用培训课程，广受客户好评；并先后与人民邮电出版社、电子工业出版社合作出版了多本专业图书，帮助数万名工程师提升了专业技术能力。客户遍布中兴通讯、研通高频、埃威航电、国人通信等多家国内知名公司，以及台湾工业技术研究院、永业科技、全一电子等多家台湾地区企业。

易迪拓培训课程列表：http://www.edatop.com/peixun/rfe/129.html

射频工程师养成培训课程套装

该套装精选了射频专业基础培训课程、射频仿真设计培训课程和射频电路测量培训课程三个类别共 30 门视频培训课程和 3 本图书教材；旨在引领学员全面学习一个射频工程师需要熟悉、理解和掌握的专业知识和研发设计能力。通过套装的学习，能够让学员完全达到和胜任一个合格的射频工程师的要求…

课程网址：http://www.edatop.com/peixun/rfe/110.html

ADS 学习培训课程套装

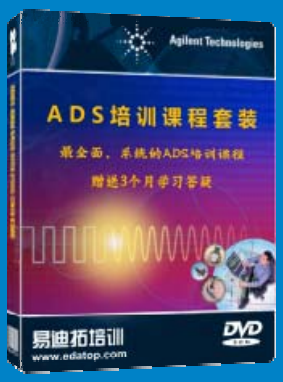

该套装是迄今国内最全面、最权威的 ADS 培训教程，共包含 10 门 ADS 学习培训课程。课程是由具有多年 ADS 使用经验的微波射频与通信系统设计领域资深专家讲解，并多结合设计实例，由浅入深、详细而又全面地讲解了 ADS 在微波射频电路设计、通信系统设计和电磁仿真设计方面的内容。能让您在最短的时间内学会使用 ADS，迅速提升个人技术能力，把 ADS 真正应用到实际研发工作中去，成为 ADS 设计专家...

课程网址： http://www.edatop.com/peixun/ads/13.html

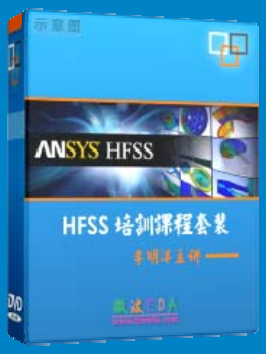

HFSS 学习培训课程套装

该套课程套装包含了本站全部 HFSS 培训课程，是迄今国内最全面、最专业的 HFSS 培训教程套装，可以帮助您从零开始，全面深入学习 HFSS 的各项功能和在多个方面的工程应用。购买套装，更可超值赠送 3 个月免费学习答疑，随时解答您学习过程中遇到的棘手问题，让您的 HFSS 学习更加轻松顺畅…

课程网址：http://www.edatop.com/peixun/hfss/11.html

CST 学习培训课程套装

该培训套装由易迪拓培训联合微波 EDA 网共同推出，是最全面、系统、专业的 CST 微波工作室培训课程套装，所有课程都由经验丰富的专家授课，视频教学，可以帮助您从零开始，全面系统地学习 CST 微波工作的各项功能及其在微波射频、天线设计等领域的设计应用。且购买该套装，还可超值赠送 3 个月免费学习答疑…

课程网址：http://www.edatop.com/peixun/cst/24.html

HFSS 天线设计培训课程套装

套装包含 6 门视频课程和 1 本图书，课程从基础讲起，内容由浅入深，理论介绍和实际操作讲解相结合，全面系统的讲解了 HFSS 天线设计的全过程。是国内最全面、最专业的 HFSS 天线设计课程，可以帮助您快速学习掌握如何使用 HFSS 设计天线，让天线设计不再难…

课程网址：http://www.edatop.com/peixun/hfss/122.html

13.56MHz NFC/RFID 线圈天线设计培训课程套装

套装包含 4 门视频培训课程，培训将 13.56MHz 线圈天线设计原理和仿真设计实践相结合，全面系统地讲解了 13.56MHz 线圈天线的工作原理、设计方法、设计考量以及使用 HFSS 和 CST 仿真分析线圈天线的具体操作，同时还介绍了 13.56MHz 线圈天线匹配电路的设计和调试。通过该套课程的学习，可以帮助您快速学习掌握 13.56MHz 线圈天线及其匹配电路的原理、设计和调试…

详情浏览：http://www.edatop.com/peixun/antenna/116.html

我们的课程优势：

※ 成立于 2004 年，10 多年丰富的行业经验，

※ 一直致力并专注于微波射频和天线设计工程师的培养，更了解该行业对人才的要求

※ 经验丰富的一线资深工程师讲授，结合实际工程案例，直观、实用、易学

联系我们：

※ 易迪拓培训官网：http://www.edatop.com

※ 微波 EDA 网：http://www.mweda.com

※ 官方淘宝店：http://shop36920890.taobao.com